The Astrophysical Journal, 626:411–424, 2005 June 10
© 2005. The American Astronomical Society. All rights reserved. Printed in U.S.A.

UVBLUE: A NEW HIGH-RESOLUTION THEORETICAL LIBRARY OF ULTRAVIOLET STELLAR SPECTRA

L. H. Rodríguez-Merino, M. Chavez,[1] and E. Bertone
INAOE, Luis Enrique Erro 1, 72840, Tonantzintla, Puebla, Mexico; lino@inaoep.mx, mchavez@inaoep.mx, ebertone@inaoep.mx

and

A. Buzzoni
INAF–Osservatorio Astronomico di Bologna, Via Ranzani 1, 40127 Bologna, Italy; buzzoni@bo.astro.it
Received 2004 October 13; accepted 2005 February 11

ABSTRACT

We present an extended ultraviolet-blue (850–4700 Å) library of theoretical stellar spectral energy distributions computed at high resolution, $\lambda/\Delta\lambda = 50{,}000$. The UVBLUE grid, as we named the library, is based on LTE calculations carried out with ATLAS9 and SYNTHE codes developed by R. L. Kurucz and consists of nearly 1800 entries that cover a large volume of the parameter space. It spans a range in $T_{\rm eff}$ from 3000 to 50,000 K, the surface gravity ranges from $\log g = 0.0$ to 5.0 with $\Delta\log g = 0.5$ dex, while seven chemical compositions are considered: $[{\rm M/H}] = -2.0,\ -1.5,\ -1.0,\ -0.5,\ +0.0,\ +0.3$, and +0.5 dex. For its coverage across the Hertzsprung-Russell diagram, this library is the most comprehensive one ever computed at high resolution in the short-wavelength spectral range, and useful application can be foreseen for both the study of single stars and in population synthesis models of galaxies and other stellar systems. We briefly discuss some relevant issues for a safe application of the theoretical output to ultraviolet observations, and a comparison of our LTE models with the non-LTE (NLTE) ones from the TLUSTY code is also carried out. NLTE spectra are found, on average, to be slightly "redder" compared to the LTE ones for the same value of $T_{\rm eff}$, while a larger difference could be detected for weak lines, which are nearly wiped out by the enhanced core emission component in case of NLTE atmospheres. These effects seem to be magnified at low metallicity (typically $[{\rm M/H}] \lesssim -1$). A match with a working sample of 111 stars from the *IUE* atlas, with available atmosphere parameters from the literature, shows that UVBLUE models provide an accurate description of the main mid- and low-resolution spectral features for stars along the whole sequence from the B to ~G5 type. The comparison sensibly degrades for later spectral types, with supergiant stars that are in general more poorly reproduced than dwarfs. As a possible explanation of this overall trend, we partly invoke the uncertainty in the input atmosphere parameters to compute the theoretical spectra. In addition, one should also consider the important contamination of the *IUE* stellar sample, where the presence of binary and variable stars certainly works in the sense of artificially worsening the match between theory and observations.

Subject headings: stars: atmospheres — ultraviolet: stars

1. INTRODUCTION

The study of the ultraviolet (UV) properties of stars has been an expanding field of research in the last few decades, following the pioneering space missions of the *Voyager*, *OAO*, and *IUE* satellites, in the 1970s. In more recent years, the two Astro missions with the Hopkins Ultraviolet Telescope (HUT) and the Goddard High Resolution Spectrograph (GHRS), on board the *Hubble Space Telescope* (*HST*), opened the way to new-generation instrumentation for space observation at short wavelengths. The Space Telescope Imaging Spectrograph (STIS), which replaced GHRS, was carrying out observations of high-resolution spectra in the near-UV range (1900–3300 Å), while the *Far Ultraviolet Spectroscopic Explorer* (*FUSE*) has pushed the far-UV (912–1900 Å) observations down to the Lyman limit with an unprecedented resolution ($R = \lambda/\Delta\lambda \approx 20{,}000$; Moos et al. 2000). On the side of UV imaging, a fresh wealth of data is coming from the *GALEX* space mission, which collects observations of stars and galaxies in two adjacent photometric bands over the wavelength range 1350–2800 Å.

To cope with these striking advances in the observational capabilities, we now urge improved theoretical tools to carry out the analysis of stellar spectra at comparable accuracy and resolution (see, on this line, an early exploratory discussion of Leckrone et al. 1990). In addition, a homogeneous and complete collection of synthetic spectral energy distributions (SEDs) of stars is also a basic demand for population synthesis codes (cf., e.g., Buzzoni 1989; Bressan et al. 1994; Worthey 1994; Leitherer et al. 1999; Vazdekis 1999; Bruzual & Charlot 2003; Gonzalez Delgado et al. 2005), so extensively used to model the UV emission of high-redshift galaxies, as seen at optical wavelengths with ground telescopes (Pettini 2002; Buzzoni 2003).

A notable, but forcedly palliative, input in this sense has come from the empirical compilations of UV spectra, the most comprehensive one probably being the Wu et al. (1983) stellar atlas, based on the original *IUE* archive and covering the range 1200–3300 Å. Shortward of Lyα, Pellerin et al. (2002) also presented an important database of galactic OB-type stars observed with *FUSE*, while Walborn et al. (2002) extended this library to the metal-poor range, including stars of the Magellanic Clouds.

As for the main optical data collections (e.g., the STELIB library of Le Borgne et al. [2003] or the Gunn & Stryker [1983], Jacoby et al. [1984], and Pickles [1985] atlases), however, a recognized drawback of UV empirical libraries is that observations can hardly assure any homogeneous and complete coverage of the stellar parameters; quite often these libraries have nonnegligible discrepancies in the determination of the distinctive

[1] Visiting Astronomer, Steward Observatory and Lunar and Planetary Laboratory, University of Arizona, Tucson, AZ 85721.

atmosphere parameters to label target stars (see, as an illuminating example, the compilation of chemical abundances as reported by Cayrel et al. 1997).

In this respect, theoretical libraries could play a key role, as model atmospheres can be computed for virtually any desired combination of parameters. Moreover, thanks to more sophisticated numerical techniques and computer performances, calculations can now rely on complete and accurate opacities, leading to a more refined treatment of line blanketing (see, e.g., Lanz & Hubeny 2003), also accounting for nonstandard physical conditions such as relaxed hydrostatic or thermodynamical equilibrium (Hauschildt et al. 1995; Schaerer & de Koter 1997; Gonzalez Delgado & Leitherer 1999; Kudritzki & Puls 2000).

A general weak point for most of the current theoretical data sets, however, is a quite poor spectral resolution,[2] and this poses an obvious limitation when matching the high-resolution observations now available. A tentative effort to overcome this gap is that of Brown et al. (1996), who provided a synthetic grid of about 1500 UV spectra at an increased resolution of 3 Å between 900 and 1800 Å; this data set, however, is especially tuned to old (low-mass) stars, with a limited coverage of stellar parameters and based on some time-saving approximations in the computing algorithm.

All previous arguments gave us a strong motivation to further tackle the problem of the UV emission of stars, and we embark, in this paper, on a systematic computation of synthetic SEDs at high spectral resolution ($R = 50{,}000$) in this wavelength range. The UVBLUE grid, as we named our theoretical library, is based on the Kurucz (1993a) code and is primarily aimed at complementing stellar libraries in the ultraviolet-blue spectral range currently in use for stellar populations studies. Nevertheless, we also foresee a fruitful use of our output for diagnostics of individual stars, especially when optical information can be added to the UV data, and suitably matched with model grids at longer wavelength in order to determine the fundamental parameters like effective temperature ($T_{\rm eff}$), surface gravity ($\log g$), and chemical composition ([M/H]) by matching observed spectra (see, e.g., Bertone et al. 2004).

We arrange our discussion, presenting in § 2 a brief summary of the Kurucz original models atmospheres that served as a main reference for our calculation. In § 3 we list the main computational characteristics we have considered when using SYNTHE spectrum synthesis codes, and we present the resulting atlas. Section 4 is a critical overview of some physical issues for proper use of our theoretical library in comparison with UV observations. A direct test is carried out in this section, matching the *IUE* low-resolution spectra of an extended sample of stars of different spectral types. Our relevant conclusions are finally summarized in § 5, together with some hints for future work.

2. THE KURUCZ MODEL ATMOSPHERES

The reference code for our atmosphere model calculations is ATLAS9, which has been constructed by Kurucz (1993a) in the so-called classical-model approximation, namely, assuming plane-parallel atmosphere layers in hydrostatic and local thermodynamic equilibrium (LTE), and with fixed chemical composition. The physical variables are constant with time; in addition, convective equilibrium is accounted for through the mixing-length theory (Böhm-Vitense 1958) with a mixing-length to pressure scale-height ratio of $l/H_p = 1.25$. The current version of ATLAS9 is the result of a long-standing upgrade process of the original version of the code (Kurucz 1979). As a major improvement over the years, special care has been devoted to a refined treatment of UV emission in the model atmospheres, both in terms of better input physics and computational performances. In particular, three important upgrades have been introduced in the current version of the code.

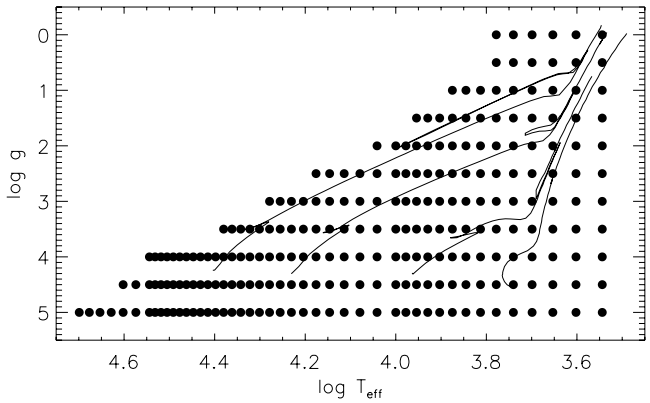

FIG. 1.—Parameter space covered by the UVBLUE grid (*dots*) overplotted with a set of solar chemical composition evolutionary tracks for 1, 2, 5, and 10 $M_\odot$ (Girardi et al. 2000; Salasnich et al. 2000).

1. Inclusion and correction of iron and iron-peak element opacities (Kurucz 1992) has been performed. Currently, the line lists constructed comprise nearly 60 million lines of atoms and diatomic molecules, of which 42 million correspond to iron group species. The line lists include up to nine ionization stages (Kurucz 1995).

2. Atmosphere spatial resolution has been increased to 72 layers, and calculations encompass a range in the Rosseland optical depth from $\log \tau_{\rm Ross} \sim 2$ "outward" to $\log \tau_{\rm Ross} \sim -7$.

3. In addition to the standard mixing-length theory, convection could be accounted for in the models according to the so-called approximate overshooting (Castelli et al. 1997). However, while this approach is found to provide a better fit to the solar spectrum, it is a still controversial question whether it definitely holds, in general, for real stars other than the Sun (Castelli et al. 1997). For this reason we eventually relied on the standard mixing-length treatment for our models.

For the sake of homogeneity, we decided to recompute a substantial portion of Kurucz's grid of model atmospheres using John Lester's modified version of ATLAS9 adapted to run under Unix systems.[3] The parameter space covered by our library (and for which we provide a high-resolution synthetic spectrum) is summarized in Figure 1. The plot displays the model grid for solar metallicity, compared in the $\log g$ versus $\log T_{\rm eff}$ plane with four reference tracks reporting the evolution of stars of 1, 2, 5, and 10 $M_\odot$, from Girardi et al. (2000) and Salasnich et al. (2000). One sees that the effective temperature is explored over the range $T_{\rm eff} = 3000 \rightarrow 50{,}000$ K, with step of 500, 1000, and 2500 K in the intervals 3000–10,000, 10,000–35,000, and 35,000–50,000 K, respectively; surface gravity is in the range $\log g = 0.0 \rightarrow 5.0$ dex, with steps of 0.5 dex, and seven metallicity values are included, namely, [M/H] = −2.0, −1.5, −1.0, −0.5, +0.0 (solar), +0.3, and +0.5 dex. The metal mix is

[2] The currently available Kurucz SEDs, for instance, sample the UV spectral range at a 10 Å step.

[3] A downloadable version of Lester's program is available at ftp://ccp7.dur.ac.uk/library.ccp7.

TABLE 1
DISTINCTIVE FEATURES OF THE UVBLUE SPECTRAL LIBRARY

Parameter	Value
$T_{\rm eff}$	3000–50,000 K
[M/H]	−2.0, −1.5, −1.0, −0.5, + 0.0, + 0.3, +0.5 dex
log g	0.0–5.0 dex at steps of 0.5 dex
Microturbulent velocity (ξ)	2 km s^{-1}
Wavelength range	850–4700 Å
Resolving power, $R = \lambda/\Delta\lambda$	50,000
Number of spectra	1770
Wavelength points per spectrum	342,016

solar-scaled, assuming the Anders & Grevesse (1989) chemical abundances for the Sun. All models have been computed with a microturbulent velocity $\xi = 2$ km s^{-1}.

3. UVBLUE: COMPUTATIONAL CHARACTERISTICS OF SYNTHETIC SPECTRAL ENERGY DISTRIBUTIONS

The whole database of stellar atmospheres accounted for in our work amounts to 1770 models. For each of these we have computed a high-resolution synthetic spectrum resolving the transfer equation by means of the series of codes SYNTHE, developed by Kurucz (1993b), and also conveniently modified in their Unix version by John Lester.[4] In our calculations we included all the atomic lines available in the Kurucz (1992) database with empirically determined atomic constants plus all the diatomic molecular lines (namely, C_2, CN, CO, H_2, SiO, CH, NH, OH, MgH, and SiH) *except* the TiO molecule, with its nearly 37 million lines. We also excluded the "predicted" lines, that is, those lines that ostensibly generate from theoretical atomic transitions but are thus far undetected in the observed solar spectrum (Kurucz 1992; see also E. Bertone et al. 2005, in preparation, for a further discussion on this subject), as well as the very weak absorption lines, that is, those with residual intensity of less than 0.1% with respect to the continuum. This cut is justified by the fact that these weak features would barely be detectable even with the highest reachable resolution in observed UV spectra.

These simplifications in the SYNTHE code resulted in a big time savings, greatly speeding up the synthesis of stellar SED and allowing us to maintain the CPU time for the full theoretical library within reasonable limits. Quite importantly, note that by neglecting the TiO contribution we only very marginally affect the reliability of our output, as this molecule is expected to become a prevailing contributor at optical/red wavelength in M-type stars cooler than 4000 K. At these low temperatures, the UV emission of stars drops at nominal values (a fraction much less than 0.1% of the bolometric luminosity is emitted shortward of 3000 Å by late-type stars; see Buzzoni 2002).

The main computational characteristics of UVBLUE spectral library are summarized in Table 1; we recall here only the two basic features.

1. *Resolving power:* $R = 50{,}000$ *over the full library.*—This high resolution represents a substantial increase with respect to previous calculations for such a wide coverage in stellar parameters. It stands above the resolution capabilities of most current and past UV-space missions. In fact, the only instruments that have provided spectra of comparable resolution are GHRS and STIS, which reach up to $R = 100{,}000$ when used with the echelle grating setup.

2. *Wavelength interval: from* 850 *to* 4700 Å.—This interval encloses most of the UV range, with the only exception the extreme ultraviolet (EUV; 100 Å $\leq \lambda \leq$ 850 Å). To ease a further match, we also assured a 1200 Å overlap with BLUERED, the blue-optical spectral grid of E. Bertone et al. (2005, in preparation), that self-consistently complements the present work at larger wavelength.[5]

Figures 2 and 3 display some illustrative examples of the UVBLUE library in selected spectral regions. The 912 Å Lyman break is explored in Figure 2 for O-B stars of solar metallicity and log $g = 5.0$ dex. On the plot we can also recognize the features of C III, N III, C II, and Si IV at 977, 991, 1036, and 1128 Å, respectively. The interesting wavelength interval around the strong Mg II doublet at 2800 Å is also displayed in the three panels of Figure 3 for different parameter sequences as indicated in each plot. Together with the Mg doublet, it is also evident in the figure the contribution of Mg I features around 2852 Å, as well as the blend of several Fe I and Fe II features at about

[4] Our calculations have been mainly carried out with a SUN ULTRA 10 computer at the Instituto Nacional de Astrofisica Optica y Electronica, Puebla, Mexico.

[5] The full set of high-resolution SEDs of UVBLUE and the complementary optical atlas BLUERED by E. Bertone et al. (2005, in preparation) are available upon request from the authors or through the dedicated Web sites http://www.bo.astro.it/~eps/uvblue/uvblue.html and http://www.inaoep.mx/~modelos/uvblue/uvblue.html.

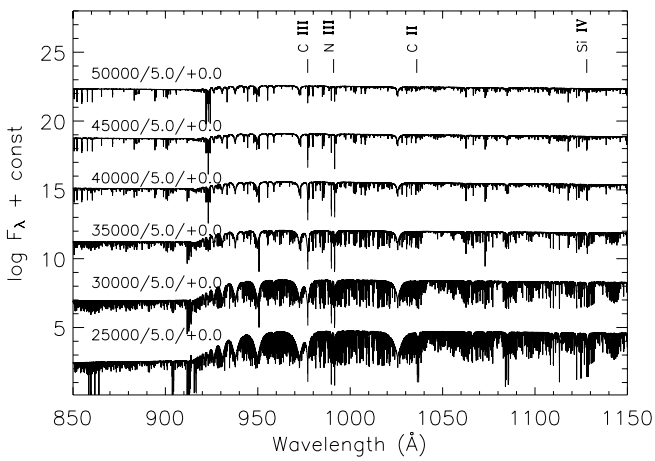

FIG. 2.—High-resolution ($R = 50{,}000$) synthetic spectra around the 912 Å Lyman break region [with sequence notation: ($T_{\rm eff}$/log g/[M/H]), as labeled for each plot]. As an illustrative example, the figure explores the trend of the break vs. $T_{\rm eff}$ for hot O-B stars of solar metallicity and log $g = 5$ dex. A number of other interesting features, such as those of C III, N III, C II, and Si IV at 977, 991, 1036, and 1128 Å, respectively, can also be recognized in the plots.

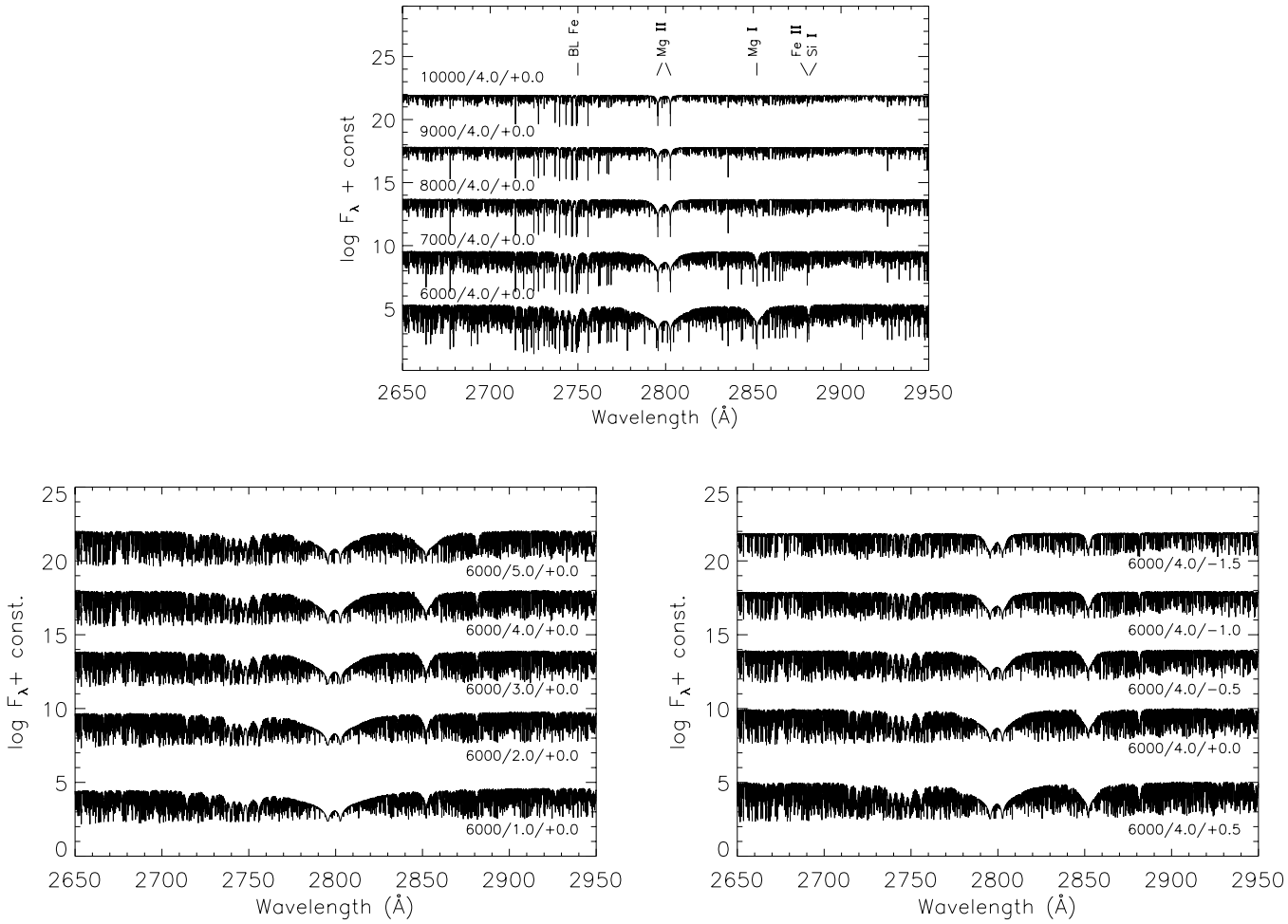

FIG. 3.—High-resolution ($R = 50{,}000$) synthetic spectra in the wavelength region around 2650–2950 Å, for different choices of stellar fundamental parameters. The explored region includes the strong Mg II doublet at 2795 and 2803 Å, very prominent in mid-F to early G-type stars and in early-type systems. *Upper panel:* the trend of SED vs. $T_{\rm eff}$ for synthetic spectra of solar metallicity and $\log g = 4.0$ dex. *Left bottom panel:* Same, but exploring the SED variation vs. surface gravity for synthetic spectra with $T_{\rm eff} = 6000$ K and [M/H] = 0.0. *Right bottom panel:* Sequence of spectra for different chemical composition, adopting $T_{\rm eff} = 6000$ K and $\log g = 4.0$ dex.

2750 Å. The Fe II and Si I lines at 2880 and 2881 Å can also be distinguished.

4. COMPARING WITH THE OBSERVATIONS

A full comparison of our theoretical output and the observed SED of real stars along the whole spectral-type sequence is the obvious (and mandatory) step of assessing the robustness of our results and probing the accuracy of theoretical spectra in reproducing the main distinctive features as observed in stars. Before carrying out this comparison, however, it is important to consider some relevant aspects that deal with the input physics of our models and should be kept in mind when matching observations.

4.1. *Caveats*

As a first substantial characteristic of our library, we are dealing with models in hydrostatic equilibrium; consequently, they should not be compared with observed spectra in wavelength regions that form in the winds of hot atmospheres. This is the case, for instance, of the strong C IV line at 1550 Å that shows a prominent P Cygni profile in main-sequence stars earlier than O7 or B0 in lower gravity objects.

Second, we have only considered one value for microturbulent velocity, $\xi = 2$ km s^{-1} (i.e., the canonical value in the Kurucz atmospheres). Non-LTE (NLTE) analyses of high-resolution spectra for early-type stars in the SMC observed with STIS and the Anglo-Australian Telescope (Bouret et al. 2003) indicate that values of ξ as high as 10 km s^{-1} might be more appropriate for the observed physical conditions. For late- and intermediate-type stars various authors claim that more suitable values for ξ are in the range 1.0–2.5 km s^{-1} depending on surface gravity (e.g., Barbuy et al. 2003). We plan to compute synthetic spectra for other values of ξ; however, we anticipate that its effects on most lines will be negligible unless very high resolution is considered. To illustrate this statement, in addition to the standard case, we have computed in Figure 4 three additional models with microturbulent velocities of $\xi = 0$, 4, and 8 km s^{-1}. For the comparison we selected the region around 1300 Å, dominated by Si II, Si III, and O I lines. The spectra are for a $T_{\rm eff} = 14{,}000$ K star with $\log g = 4.0$ dex, a combination that should maximize the blend strength of these absorption features when seen in low-dispersion spectra (Fanelli et al. 1992).

Third, we have to make sure that spectral resolution in the grid and in observational data are compatible. An illustrative example is shown in Figure 5 for the same wavelength interval of Figure 4 and for the Lyβ region at about 1030 Å. By means of Gaussian filter convolution, we degraded the spectra to four

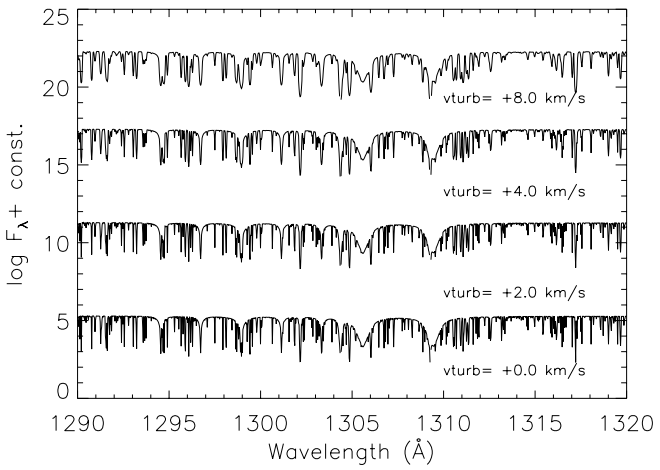

FIG. 4.—Effect of microturbulent velocity on Si/O spectral features in the wavelength interval 1290–1320 Å. The same synthetic spectrum for a $T_{\rm eff}$ = 14,000 K star with $\log g = 4.0$ dex and solar metallicity is computed by changing the value of ξ, as labeled on the plots.

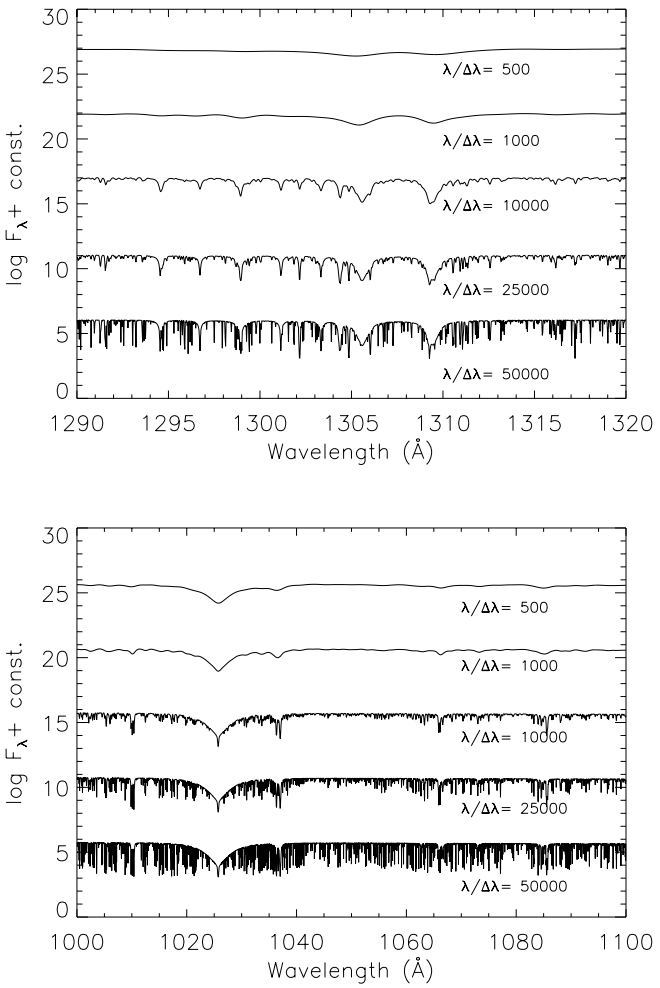

FIG. 5.—Illustrative example of the effects of instrumental resolution ($R = \lambda/\Delta\lambda$), on a spectrum with ($T_{\rm eff}$, $\log g$, [M/H]) = (15,000 K, 4.0 dex, +0.0 dex) for the wavelength region of Fig. 4 (*upper panel*), and for the Lyβ region about 1000–1100 Å (*lower panel*). The original $R = 50{,}000$ spectra have been degraded by convolution with a Gaussian kernel.

different resolutions, that is, $R = 500$, 1000, 10,000, and 25,000. Note that at the *IUE* low-resolution mode (i.e., $R \simeq 250$ at 1500 Å), most of the features would definitely be washed out, and things could get even worse at the nominal resolution of the original Kurucz grid of spectra, where $R \simeq 150$ at 1500 Å.

Fourth, our calculations do not include the effects of rotational velocity. While a vast majority of late-type stars do not show any large projected rotational velocity, we know that most early-type stars are severely affected by rotation-reaching values of $V \sin i$ up to 500 km s^{-1}. Recently, Glebocki & Stawikowski (2000) presented a compilation of over 17,000 measurements of $V \sin i$ for nearly 12,000 stars that complement previous catalogs (Uesigi & Fukuda 1982). In order to illustrate the overall dependence of $V \sin i$ on effective temperature and surface gravity, we plot in Figure 6 the $V \sin i$ distribution versus spectral type for four different luminosity classes. Only the subset of "normal" stars is considered in the plot, that is, excluding white dwarfs, Wolf Rayet, binary stars, etc. Evidently, the importance of rotation when comparing observed and UVBLUE spectra will depend on how the Doppler broadening compares with instrumental resolution.

Fifth, late-type stars are recognized to display some chromospheric activity to a different extent. Nonradiative heating in the upper atmosphere of F- to M-type stars, through acoustic waves in F0–F5 stars and magnetohydrodynamic mechanisms for later types (Böhm-Vitense et al. 2001 and references therein), causes a turnover in the temperature stratification, $T(\tau)$. This temperature distribution has important effects on the SED at short wavelength as it could trigger prominent emission lines such as, for instance, the strong Mg II doublet at 2800 Å (e.g., Blanco et al. 1982) and an overall enhancement in the UV continuum (Franchini et al. 1998). Classical models in general, and Kurucz's models in particular, do not account for this phenomenon, since temperature decreases monotonically in the outermost atmosphere layers.

4.2. *LTE versus NLTE*

It has been widely discussed in the literature that deviations from LTE are to be expected for hot stars and the cores of strong lines in stars of intermediate type (Mihalas 1972). However, it has also been demonstrated that at low resolution the agreement between LTE and NLTE model fluxes is good, and that comparison of far-UV and mid-UV observational data with LTE model fluxes also results in good agreement (Morales et al. 2000). At high resolution such a comparison has been anticipated by Lanz & Hubeny (2003) but not yet quantitatively assessed.

As the whole UVBLUE spectral library has been computed under the assumption of LTE, it may be of some interest to compare the ATLAS9 results with the corresponding output for NLTE codes. Here we considered in particular two representative sets of stellar parameters with ($T_{\rm eff}$, $\log g$) = (40,000 K, 4.5 dex) and different metallicity, namely, [M/H] = 0.0 dex (solar) and −2.0 dex. The NLTE models and theoretical SEDs have been extracted from the OSTAR2002 grid (Lanz & Hubeny 2003), based on line-blanketed model atmospheres computed with TLUSTY (Hubeny & Lanz 1992) under the condition of hydrostatic equilibrium. Available spectral fluxes cover the wavelength region from 45 Å to 300 μm at a resolution $R \simeq 40{,}000$, assuming a value of $\xi = 10$ km s^{-1}. In order to make the data sets mutually consistent, we have recalculated the corresponding ATLAS9 spectra for the same microturbulent velocity and wavelength resolution.

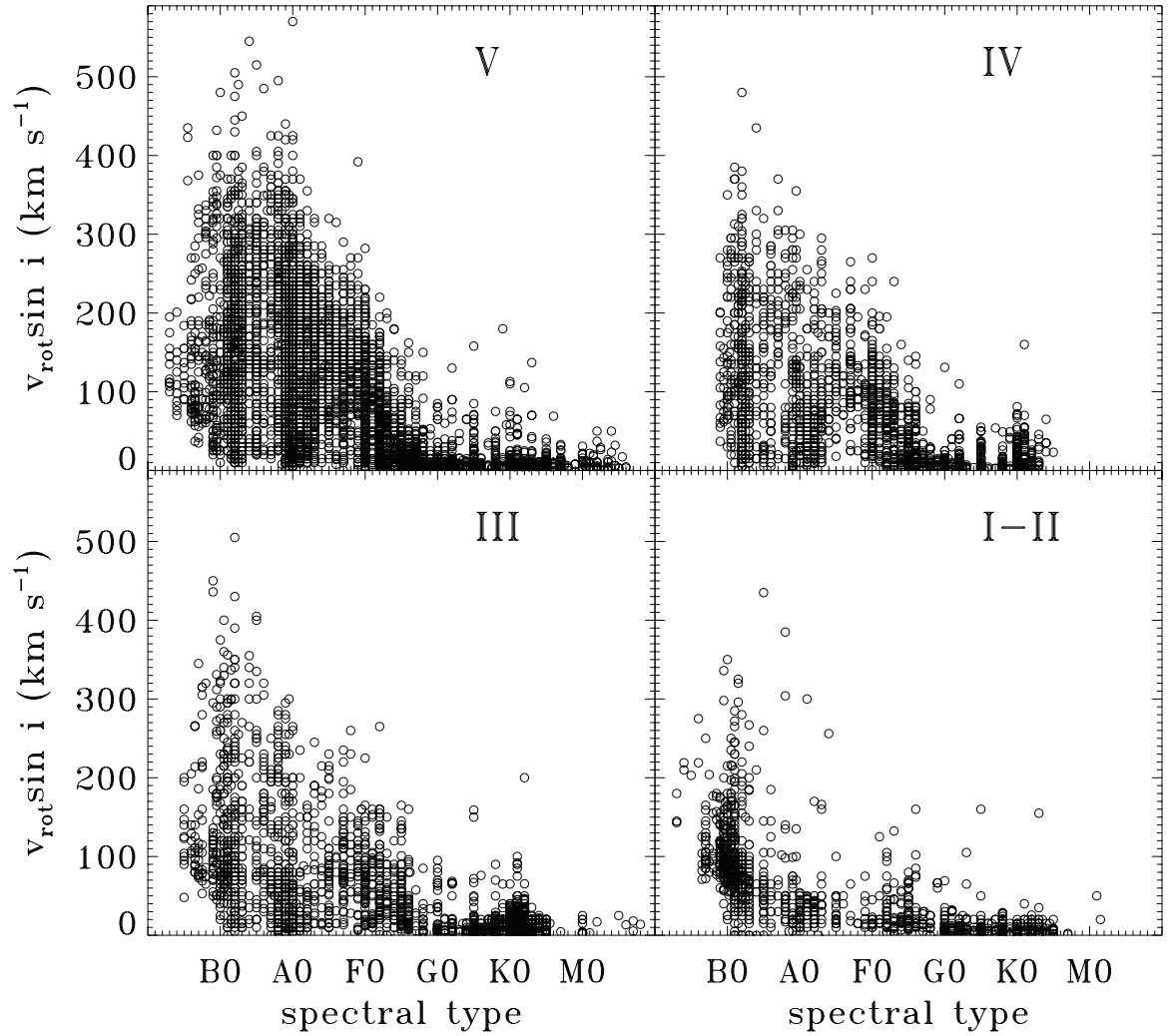

FIG. 6.—Distribution of projected rotational velocity $V \sin i$ vs. spectral type and luminosity class. Data are from the Glebocki & Stawikowski (2000) catalog, including only normal stars.

The temperature structure of ATLAS9 and TLUSTY model atmospheres is compared in the upper panels of Figure 7. Although no obvious interpretative scheme can be invoked to explain the overall differences in the LTE versus NLTE properties, the figure helps to assess some relevant features directly dealing with the different temperature stratification in the two sets of atmospheres. As a major issue, one sees that, for the same value of $T_{\rm eff}$, the outer structure of the TLUSTY models strongly modulates with metallicity, with a temperature turnover growing at metal-poor abundance; this effect can also be recognized in the original models of Kudritzki (1976). Typically, temperature inversion begins to appear in $[{\rm M/H}] \lesssim -1$ models (see Fig. 4 in Lanz & Hubeny 2003) and involves the $\log \tau_{\rm ROSS} \lesssim -2$ atmosphere layers.

On the other hand, when $\tau_{\rm ROSS}$ approaches unity, another important feature seems to characterize NLTE models. Close to the photosphere region, in fact, the NLTE temperature profile appears cooler, in general, compared with the corresponding LTE case. The size of this temperature "dip" (cf. the temperature residuals in Fig. 7) depends on the detailed physical treatment of helium opacity (see, e.g., the interesting experiments of Kudritzki 1976 and Werner 1988), but to a more or less pronounced extent, it seems to be a quite general feature for NLTE atmospheres. As a consequence, for fixed value of $T_{\rm eff}$, NLTE models tend to be "redder" than the corresponding LTE solution because the continuum forms in a slightly cooler physical environment; this especially reflects in short-wavelength colors, like the Strömgren $u - b$, as first indicated by Kudritzki (1976). Direct evidence in the sense of a mildly depressed UV/blue continuum can also be derived from the Lanz & Hubeny (2003) SEDs, when comparing them with the Kurucz LTE models.

The composite trend of temperature stratification leads, in addition, to different behavior of high-resolution features in the SED of stars. As far as "weak" absorption lines are concerned (that is those mainly generating in the innermost regions of star atmospheres), the core emission component induced by the temperature turnover of the external NLTE layers should likely act in the sense of "filling" out the features. This would be especially evident at metal-poor regimes, as can be easily recognized in the $[{\rm M/H}] = -2$ synthetic spectrum of Figure 7 (*right panels*). On the contrary, for those strong (or saturated) absorption features, whose core forms at the optical depth about the region of the temperature dip, we would rather expect a slightly increased equivalent width for NLTE models, again as a result of a cooler temperature environment. This is the case, for instance, of some Si IV and C IV lines (see Fig. 7, *left panel*), or hydrogen Balmer absorptions, like Hγ at 4340 Å, or the He II absorption at 4542 Å, as shown by Kudritzki (1976).

The UV SED of late-type stars is also affected by deviations from LTE. In addition to the still controversial "missing solar

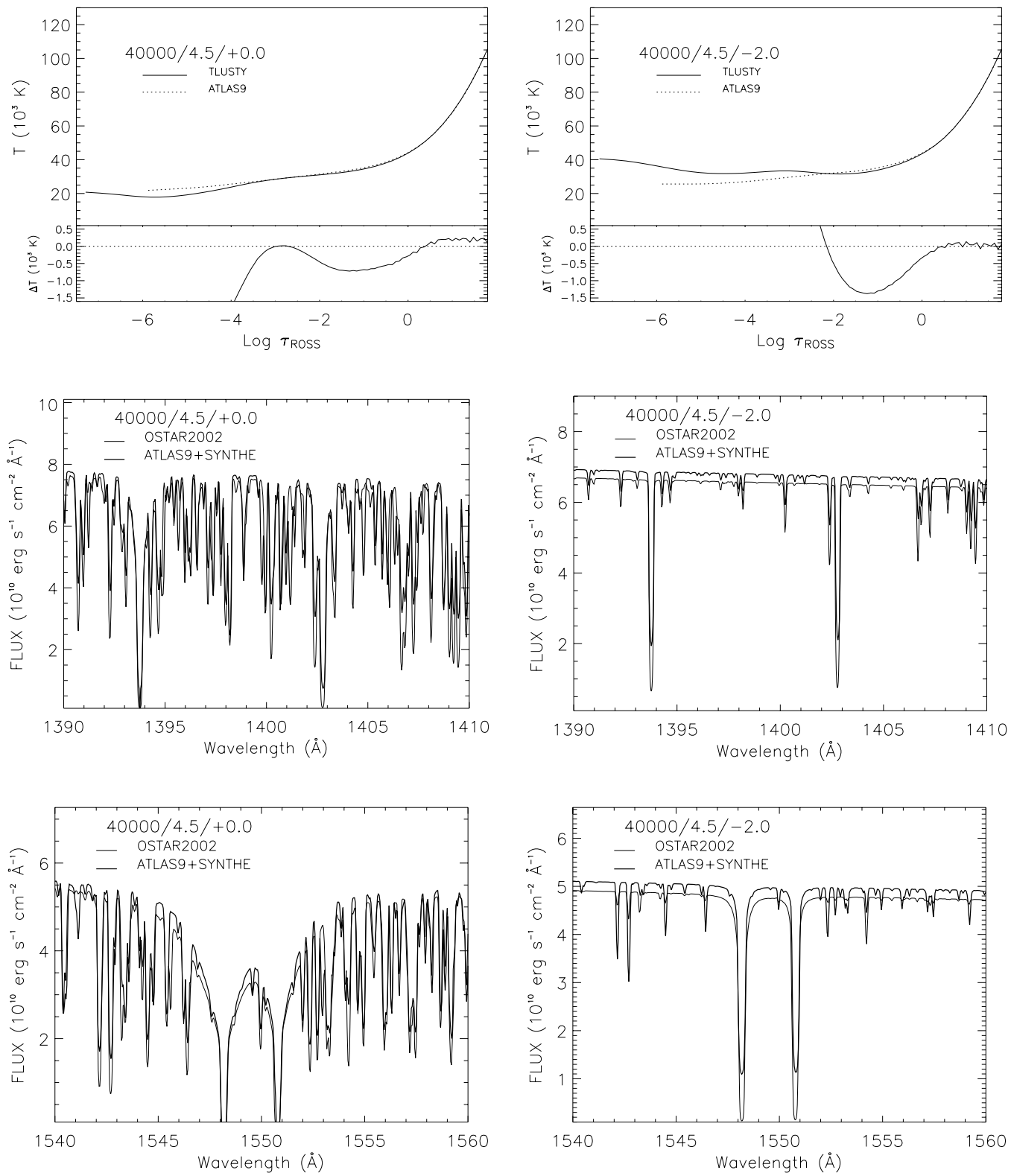

FIG. 7.—Comparison of LTE and NLTE atmosphere models and synthetic spectra. *Upper panels*: The upper box displays the temperature profiles of four atmosphere models, two models calculated with ATLAS9 and the other two from the OSTAR2002 grid. The lower box displays the residuals in the form ΔT TLUSTY-ATLAS9. *Middle panels*: High-resolution ($R \sim 40{,}000$) spectra in the wavelength region 1390–1410 Å, showing two prominent lines of Si IV. *Lower panels*: High-resolution ($R \sim 40{,}000$) spectra in the wavelength region centered on the C IV doublet about 1550 Å.

UV opacity" (Holweger 1970; Gustafsson et al. 1975), in fact, some of the disagreements found when comparing the observed and theoretical solar spectrum have been ascribed to NLTE effects. However, the recent analysis by Allende Prieto et al. (2003) indicates that the claimed discrepancy between theory and observations in the mid-UV region around 2400–2600 Å for the Sun cannot be overcome by (and actually even worsen with) NLTE calculations.

4.3. *Matching the IUE Spectral Atlas*

As we mentioned previously, the Wu et al. (1983) atlas of stellar spectra, from the *IUE* data, still remains a main reference to compare the UVBLUE theoretical output. This composite atlas has been the work-horse of numerous investigations on the calibration of stellar features in terms of stellar parameters, as well as population studies. The original sample of 170 stars has been further extended to 220 objects by Fanelli et al. (1990) by including most late-type stars and completing the sampling of spectral types, from O to M, and luminosity classes, from I to V. Many subsequent updates have further increased the number of entries, and the current Web version of the catalog[6] comprises 476 objects.

For the illustrative scope of our work, we restrained the analysis to only the 220 stars of the originally published version of the catalog (hereafter referred to as "the *IUE* atlas"). Each object of this sample has been cross-checked with the literature data, mainly relying on the Cayrel et al. (1997) catalog, in order to derive a complete set of atmosphere fundamental parameters from high-resolution spectroscopy at optical wavelength. In case of multiple determinations for the same star, the average values for $T_{\rm eff}$, $\log g$, and [M/H] have been considered (retaining, however, only those literature sources with complete estimates of *all* the three parameters), together with a measure of the nominal uncertainty from the data dispersion.

Our search procedure eventually secured complete atmosphere parameters for 111 stars of the original *IUE* atlas. For this working sample, Table 2 collects the relevant information, while the three panels of Figure 8 report the distribution of stars in spectral type, luminosity class, and metallicity. In Table 2, columns (1)–(5) give, respectively, the HD number of the star, its spectral classification (from the SIMBAD database), color excess (from the Fanelli et al. 1992 compilation), atmosphere parameters (from Cayrel et al. 1997 unless otherwise stated), and their rms (for those cases with multiple determinations in the literature).

In order to assure an accurate and homogeneous observational data set, from the updated INES/*IUE* database[7] we extracted and reprocessed all the relevant frames for stars in our sample. In particular, we considered all the available low-dispersion spectra collected in large aperture (20″) mode and with poor-quality flags affecting less than 40% of the wavelength points.[8] The number of SWP and LWP/LWR frames eventually used in our analysis is reported in columns (7) and (8) of Table 2. Wavelength calibration for the whole database was tuned up by fitting several prominent features in the spectra according to the stellar type. For example, for hot stars we mainly relied on Lyα, C IV at 1550 Å, Al II at 1617 Å etc., while for cool stars we used the blend of Si and Cr lines at 2124 Å and the Mg I line at 2852 Å. In any case, at least four lines were used for wavelength fine-tuning. For those stars with multiple observations, the fiducial SED for each star was obtained by averaging the total number of images.

The resulting mean spectrum was weighted by the errors ascribed to the flux given in the INES files. All spectra have then been corrected for Galactic reddening according to Mathis (1990); we assumed $R_V = 3.1$ and the color excess $E(B-V)$ as reported by Fanelli et al. (1992; see Table 2). Figure 9 displays an illustrative example of the SED along the spectral-type sequence for stars of different luminosity class.

The observed SED of each star in the *IUE* working sample has been matched with the theoretical spectra by interpolating the UVBLUE library according to the fiducial atmosphere parameters of Table 2. In order to allow a self-consistent comparison, the theoretical SED was then degraded to the *IUE* 6 Å wavelength resolution and rebinned at the wavelength points of the observations. The comparison was taken over a common wavelength range according to the spectral type. For hot stars this spanned the 1300–3250 Å interval, excluding the extreme UV region shortward of the Lyα line, possibly affected by interstellar absorption (Diplas & Savage 1994; Brandt et al. 1998). As emission of cooler stars drops at nominal values in the far-UV range, for late spectral types we restrained the SED comparison longward of 1650 Å for A-type objects, 2200 Å for the F-G types, and 2500 Å for K and M stars. An example of our comparison procedure, for a selected set of *IUE* stars of different spectral type, is shown in Figure 10.

A straightforward measure of the "likeness" between observed and theoretical SED directly derives from the standard deviation of the [(*IUE*)–(UVBLUE)] flux residuals (in the natural logarithm domain), defined as

$$\sigma = \sqrt{\mathrm{var}[\ln f(\lambda)_{IUE} - \ln f(\lambda)_{\rm UVBLUE}]}. \qquad (1)$$

This definition is independent of the flux offset between theoretical and observed spectra and therefore overcomes any internal uncertainty in the zero-point calibration.[9]

Figure 11 gives an overall summary of σ versus spectral type and luminosity class for the 111 stars in our working sample; the individual values of σ for each target star are also reported in column (6) of Table 2. It is evident that the rms value drastically degrades for spectral types later than G5, with supergiant stars that are in general more poorly reproduced by the UVBLUE models.

Quite importantly, we point out in this regard that our procedure does *not* search for any best fit to the *IUE* observations but simply compares the observed spectrum and the corresponding theoretical SED obtained from the fiducial atmosphere parameters of the literature. This should certainly assure an independent "acid test" for the theoretical library, although one should also be aware that any inaccurate (or incorrect) set of input fundamental parameters (and even more any uncertainty in the reddening correction) for a star could be reflected in a sensible increase of the value of σ. In addition, one should also consider

[6] See http://www-int.stsci.edu/~jinger/iue.html.

[7] Our work is based on the INES/*IUE* general archive hosted at the Mexican and Spanish distribution centers of INAOE (http://www.inaoep.mx) and LAEFF (http://ines.laeff.esa.es), respectively.

[8] Note that poor-quality flags quite frequently mark background bad pixels in the original *IUE* frames. Their presence in the extracted one-dimensional spectra does not necessarily indicate a pixel defeat. In any case, visual inspection on each single image discerned whether the spectrum was to be rejected or not.

[9] Note that our normalization procedure fully overcomes any internal uncertainty in the zero-point calibration of the INES/*IUE* database. In this regard, the claimed ~7% systematic offset of the *IUE* archive with respect to *HST*/FOS data (e.g., González-Riestra et al. 2001), for instance, has no effect on our comparison.

TABLE 2

IUE Ultraviolet Atlas

HD (1)	Spectral Type (2)	$E(B-V)$ (3)	$T_{\rm eff}$/ log g/[M/H] (4)	rms (5)	σ (6)	Number of Images SWP (7)	Number of Images LWR/LWP (8)	Remarks (9)
2151	G2 IV	0.00	5793/4.05/−0.17	71/0.25/0.10	0.34	14	3	Variable
3360	B2 IV	0.04	22180/3.92/−0.23	.../.../...	0.08	21	65	Variable
4128	K0 III	0.00	4836/2.62/0.01	86/0.22/0.12	0.79	5	4	Variable
4307	G2 V	0.00	5736/3.99/−0.32	103/0.09/0.06	0.27	0	2	...
4614	G0 V	0.00	5809/4.41/−0.23	135/0.04/0.06	0.28	4	2	Spectral binary
6203	K0 III	0.00	4560/2.96/−0.35	.../.../...	0.79	0	2	Double system
10307	G1.5 V	0.00	5845/4.35/−0.02	74/0.05/0.01	0.38	1	1	...
10380	K3 IIIb	0.00	4052/1.43/−0.29	60/0.47/0.05	0.95	1	2	...
10476	K1 V	0.00	5196/4.50/−0.20	.../.../...	0.53	2	3	Variable
10700	G8 V	0.00	5229/4.36/−0.53	125/0.36/0.11	0.38	8	3	...
10780	K0 V	0.00	5419/4.60/0.36	.../.../...	0.53	4	5	...
14802	G2 V	0.00	5917/4.30/−0.09	16/0.15/0.13	0.33	1	2	...
17081	B7 IV	0.00	12807/3.64/0.05	901/0.31/0.46	0.07	1	1	...
17709	K5 III	0.00	3880/1.42/−0.36	.../.../...	1.01	1	1	Variable
19058	M4 II	0.00	3500/0.80/0.05	.../.../...	1.17	4	7	Pulsating
19476	K0 III	0.00	4953/3.09/0.10	24/0.29/0.06	0.69	0	1	Variable
20630	G5 Vvar	0.00	5648/4.41/0.03	32/0.09/0.04	0.49	17	3	Variable
22049	K2 V	0.00	5058/4.55/−0.20	79/0.25/0.08	0.61	78	15	Variable
22879	F9 V	0.00	5838/4.15/−0.88	62/0.17/0.07	0.17	1	3	...
26630	G0 Ib	0.19	5331/1.38/0.02	159/0.13/0.21	1.24	7	2	Spectral binary
27383	F9 V	0.00	6280/4.55/0.10[a]	.../.../...	0.28	1	1	In-cluster
27561	F5 V	0.00	6700/4.33/0.04[a]	.../.../...	0.23	0	1	In-cluster
27808	F8 V	0.00	6340/4.36/0.10[a]	.../.../...	0.27	2	2	In-cluster
27836	G1 V	0.00	6120/4.65/−0.08[a]	.../.../...	0.38	3	3	Variable
28527	A6 IV	0.00	7986/4.18/0.14[b]	.../.../...	0.21	1	2	Variable
29139	K5 III	0.00	3903/1.26/−0.10	150/0.36/0.22	1.03	20	1	Variable
34816	B0.5 IV	0.00	30695/4.14/0.38	1138/0.12/0.88	0.05	19	34	...
35620	K3 IIICN	0.00	4238/1.68/−0.14	131/0.42/0.22	0.95	0	2	Double system
36512	B0 V	0.04	31500/4.13/0.25	.../.../...	0.08	2	3	...
36673	F0 Ib	0.02	7234/1.38/−0.04	208/0.33/0.08	0.20	2	1	Variable
37160	K0 IIIb	0.00	4504/2.56/−0.58	287/0.24/0.17	0.69	0	1	...
38666	O9.5 V	0.00	31790/4.00/−0.74[c]	.../.../...	0.07	15	27	Variable
38899	B9 IV	0.00	10903/4.00/0.01	75/0.14/0.09	0.08	1	1	Double system
40136	F1 V	0.03	7127/4.14/−0.13	250/0.13/0.08	0.14	3	3	...
44478	M3 III	0.00	3600/1.00/0.11	.../.../...	1.09	1	3	Variable
46328	B1 III	0.01	27720/4.00/–0.18	.../.../...	0.07	1	1	Variable
48329	G8 Ib	0.26	4592/0.81/−0.05	21/0.17/0.03	1.68	4	4	Variable
49293	K0 IIIa	0.00	4620/2.59/−0.12	.../.../...	0.80	0	2	...
54605	F8 Iab:	0.09	6222/1.00/0.35	.../0.28/0.23	0.46	6	3	Variable
54719	K2 III	0.00	4350/2.17/0.02	.../.../...	0.92	0	1	Variable
55575	G0 V	0.00	5878/4.23/−0.36	120/0.35/0.11	0.29	0	1	...
59612	A6 Ib/II	0.14	8100/1.50/0.08	.../.../...	0.19	2	2	Multiple-Star
62509	K0 IIIb	0.00	4890/2.66/0.07	78/0.30/0.27	0.71	12	5	Variable
63922	B0 III	0.11	30300/4.00/0.33	.../.../...	0.09	1	1	Double system
64606	G8 V	0.00	5139/4.08/−0.99	68/0.25/0.03	0.44	0	1	...
66141	K2 III	0.00	4250/2.29/−0.36	.../.../...	0.86	0	1	Double
69267	K4 III	0.00	4072/1.73/−0.17	211/0.14/0.10	0.99	2	1	Variable
70272	K4.5 III	0.00	3900/1.59/−0.03	.../.../...	1.00	0	1	Variable
72184	K2 III	0.00	4525/2.05/−0.05	.../.../...	0.92	0	2	...
72324	G9 III	0.00	4730/2.08/−0.10	28/0.25/0.14	0.91	0	2	...
73471	K1 III	0.00	4500/2.36/0.05	.../.../...	0.99	0	1	...
75732	G8 V	0.00	5196/4.47/0.22	.../0.06/0.10	0.69	0	1	...
76294	G9 II-II	0.00	4870/2.49/−0.01	26/0.29/0.34	0.75	2	2	...
78647	K4 Ib-II	0.07	4235/1.40/0.23	.../.../...	1.40	2	3	Variable
82328	F6 IV	0.00	6227/3.98/−0.11	245/0.30/0.10	0.21	2	3	Spectral binary
84441	G1 II	0.08	5343/2.05/−0.08	66/0.35/0.23	0.64	0	2	Variable
85503	K2 III	0.00	4501/2.37/0.16	128/0.24/0.19	0.97	0	2	...
89025	F0 III	0.00	7182/2.97/0.12[d]	.../.../...	0.16	1	1	Variable
90839	F8 V	0.00	6072/4.41/−0.23	.../.../...	0.24	2	1	Double system
95272	K1 III	0.00	4494/2.76/−0.08	407/0.27/0.16	0.87	1	1	...
99028	F4 IV	0.06	6739/3.98/0.06	.../.../...	0.22	3	2	Spectral binary
101501	G8 V	0.00	5508/4.64/−0.05	42/0.06/0.12	0.55	3	1	Variable

TABLE 2—*Continued*

HD (1)	Spectral Type (2)	$E(B-V)$ (3)	$T_{\rm eff}$/ log g/[M/H] (4)	rms (5)	σ (6)	Number of Images SWP (7)	Number of Images LWR/LWP (8)	Remarks (9)
102870	F9 V	0.00	6124/4.24/0.19	57/0.10/0.07	0.30	4	1	...
106516	F5 V	0.00	6089/4.25/−0.76	137/0.24/0.16	0.15	3	2	...
109379	G5 II	0.00	5147/2.15/0.08	31/0.07/0.27	0.69	3	2	Variable
113139	F2 V	0.01	6890/4.13/0.02[a]	.../.../...	0.17	1	1	Multiple
114710	F9.5 V	0.00	6008/4.44/0.10	103/0.06/0.12	0.30	3	2	...
115617	G5 V	0.00	5596/4.24/−0.03	5/0.25/0.01	0.43	1	2	...
117176	G4 V	0.00	5478/3.75/−0.11	.../.../...	0.43	1	1	...
125560	K3 III	0.00	4400/2.42/0.00	.../.../...	0.91	0	2	Variable
126660	F7 V	0.00	6338/4.29/−0.05	.../.../...	0.25	3	1	Variable
132345	K3 IIICN	0.00	4322/2.08/0.05	105/0.38/0.09	0.90	0	1	Double system
134083	F5 V	0.00	6632/4.50/0.10	.../.../...	0.20	2	2	Variable
137759	K2 III	0.00	4515/2.67/0.17	36/0.10/0.19	0.91	2	1	Variable
140573	K2 IIIb	0.00	4555/2.38/0.11	51/0.44/0.17	0.92	3	1	Double system
142091	K1 IVa	0.00	4800/3.37/−0.04	.../.../...	0.71	0	1	...
142373	F8 Ve	0.00	5880/4.20/−0.42	57/0.18/0.08	0.22	4	1	...
142860	F6 IV	0.00	6340/4.10/−0.13[a]	.../.../...	0.21	3	1	Varible
142980	K1 IV	0.00	4560/3.22/0.06	.../.../...	0.84	0	2	...
145328	K1 III-I	0.00	4720/3.25/−0.20	.../.../...	0.71	0	1	Variable
145675	K0 V	0.00	5265/4.49/0.26	105/0.07/0.08	0.58	0	1	...
147394	B5 IV	0.02	14868/3.81/0.00	88/0.19/0.48	0.05	5	4	Variable
150680	G0 IV	0.00	5742/3.76/−0.07	81/0.05/0.12	0.36	4	1	Spec
157244	K3 Ib-II	0.00	4582/1.30/0.50	.../.../...	1.38	1	1	...
159181	G2 Iab:	0.15	5334/1.48/0.21	56/0.14/0.10	0.95	13	3	Double system
159561	A5 III	0.00	8126/3.97/0.30[d]	.../.../...	0.22	2	3	Variable
161471	F2 Iae	0.00	7000/1.30/0.27	.../.../...	0.34	2	2	Emission
161797	G5 IV	0.00	5463/3.92/0.19	60/0.18/0.12	0.55	6	2	...
163506	F2 Ibe	0.11	6400/1.20/−0.41	.../.../...	0.26	11	9	Pulsating
173667	F6 V	0.00	6337/4.08/−0.12	64/0.25/0.14	0.23	2	1	Variable
182572	G8 IV	0.00	5658/4.15/0.35	144/0.25/0.14	0.48	2	2	Variable
185144	K0 V	0.00	5169/4.50/−0.24	37/0.14/0.01	0.47	3	4	Variable
187691	F8 V	0.00	6146/4.34/0.12	.../0.13/0.02	0.28	1	1	...
188512	G8 IV	0.00	5212/3.09/−0.03	161/1.03/0.26	0.58	1	2	Variable
193432	B9 IV	0.00	10313/3.75/0.03	289/0.27/0.21	0.08	1	1	Double system
195633	G0 Vw	0.00	5969/3.75/−1.00	249/0.07/0.14	1.34	0	1	...
198149	K0 IV	0.00	4965/3.18/−0.18	123/0.22/0.27	0.62	2	1	...
200580	F9 V	0.00	5727/3.50/−0.75	.../.../0.07	0.19	0	2	Multiple
201091	K5 V	0.00	4364/4.55/−0.05	37/0.10/0.04	0.62	14	18	Variable
201092	K7 V	0.00	3868/4.58/−0.19	133/0.13/0.26	0.47	2	14	Flare star
206778	K2 Ib	0.20	4272/1.02/0.02	129/0.16/0.18	1.45	5	2	Variable
206859	G5 Ib	0.17	4861/1.45/−0.02	27/0.30/0.04	1.20	3	1	Variable
207978	F6 IV-Vw	0.00	6233/4.03/−0.59	102/0.20/0.07	0.16	0	1	-
209750	G2 Ib	0.12	5251/1.36/0.18	92/0.12/0.12	0.86	30	1	Double system
215648	F7 V	0.00	6134/4.14/−0.32	119/0.04/0.05	0.20	1	2	...
216385	F7 IV	0.00	6144/3.93/−0.44	92/0.13/0.14	0.21	0	1	...
216956	A3 V	0.00	8760/4.20/0.20[b]	.../.../...	0.11	4	4	Variable
217877	F8 V	0.00	6000/4.50/−0.10	.../.../...	0.28	0	1	...
219134	K3 V	0.00	4695/4.48/0.01	22/0.04/0.14	0.62	1	4	Flare star
222368	F7 V	0.00	6106/4.06/−0.31[a]	116/0.19/0.13	0.22	4	2	Variable
224930	G5 Vb	0.00	5305/4.49/−0.88	189/0.13/0.19	0.28	0	2	Spectral binary

[a] Atmosphere parameters from Gray et al. (2001).
[b] Atmosphere parameters from Gardiner et al. (1999).
[c] Atmosphere parameters from Fitzpatrick & Massa (1999).
[d] Atmosphere parameters from Morossi et al. (2002).

that the *IUE* atlas actually includes a number of "peculiar" objects; a glance to column (9) of Table 2 shows that many stars are double or multiple systems, with an important fraction of spectroscopic binaries and variables. This clearly works in the sense of artificially worsening the match with the theoretical models. We could briefly sketch the relevant results of our comparison across the whole spectral-type sequence:

1. *Early-type stars: O and B*.—Most stars in this stellar group have complete SWP+LWP/R spectra, and comparison with the synthetic SED can be carried out over the full wavelength range. One of the main discrepancies with the UVBLUE models is the C IV line at 1550 Å, partly as a consequence of the physical origin of this line, strongly affected by stellar winds and mass-loss processes in massive stars. In addition, we also

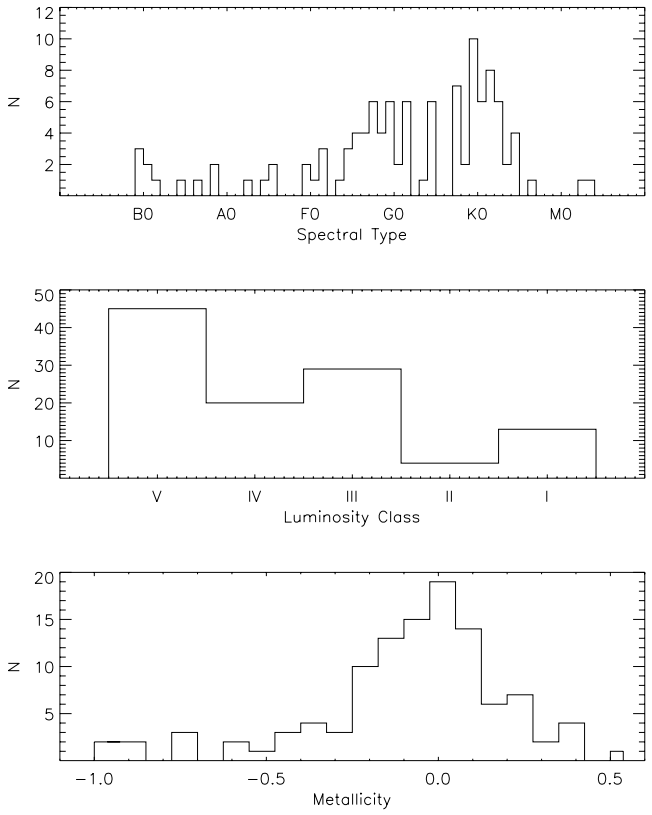

FIG. 8.—Distribution of stars in the Wu atlas as a function of spectral type, luminosity, and metallicity.

found that the O III line at 2496 Å, predicted by the models, is never detected in the observed spectra.

2. *A-type stars*.—Although to a lesser extent, for these stars the C IV line (together with the C I and Al II blend at 1670 Å) is also not well matched. As far as low-resolution features are concerned, one main source of discrepancy in late A stars is the Si I spectral break at 1530 Å, poorly reproduced by the synthetic spectra. If we neglect the spectral region around this feature the value of σ sensibly improves in at least 70% of the cases. On the other hand, it is also worth noting that, for their temperature range, A stars are the strongest far-UV emitters, and a small uncertainty in the estimated value of $T_{\rm eff}$ can therefore result in a large mismatch between the observed and theoretical SEDs (see, e.g., Cheng & Neff 2003, for a discussion on *FUSE* data for star 2 And).

3. *Intermediate-type stars: F and G*.—Only the region longward of 2200 Å was retained for these stars. Prominent metallic features of F stars are always stronger in theoretical flux, in particular the Fe II blend at 2400 Å and that of Fe I/ Si I at about 2500 Å, as well as the Mg II resonance doublet at 2800 Å and the Mg I line at 2852 Å. The Mg break around 2600 Å is also poorly reproduced by the models, with the difference increasing for decreasing gravity and effective temperature. For G stars, chromosphere activity becomes increasingly important, in most cases partially filling the Mg II doublet with a core emission. In general, the 2400–2700 Å spectral region remains the most problematic one (see Fig. 10, *lower left panel*) confirming the Allende Prieto et al. (2003) hints for a missing Mg I opacity, according to their mid-UV data of the Sun collected during the *UARS* satellite mission.

Curiously enough, all three striking outliers in Figure 11 are G-type stars, namely:

a) *HD 26630*.—A G0 supergiant with enhanced far-UV emission. The star is reported in the SIMBAD database as a spectroscopic binary ($P = 283.3$ days) and Parsons & Ake (1998) decomposed the *IUE* spectrum, isolating the contribution of a hot companion of spectral type B9.

b) *HD 48329*.—According to SIMBAD, this G8 supergiant shows microvariability and the HR catalog reports a strong P Cygni effect for the He 10830 Å infrared line. The *IUE* spectrum shows a moderate UV excess compared to the theoretical SED according to the fiducial atmosphere parameters,

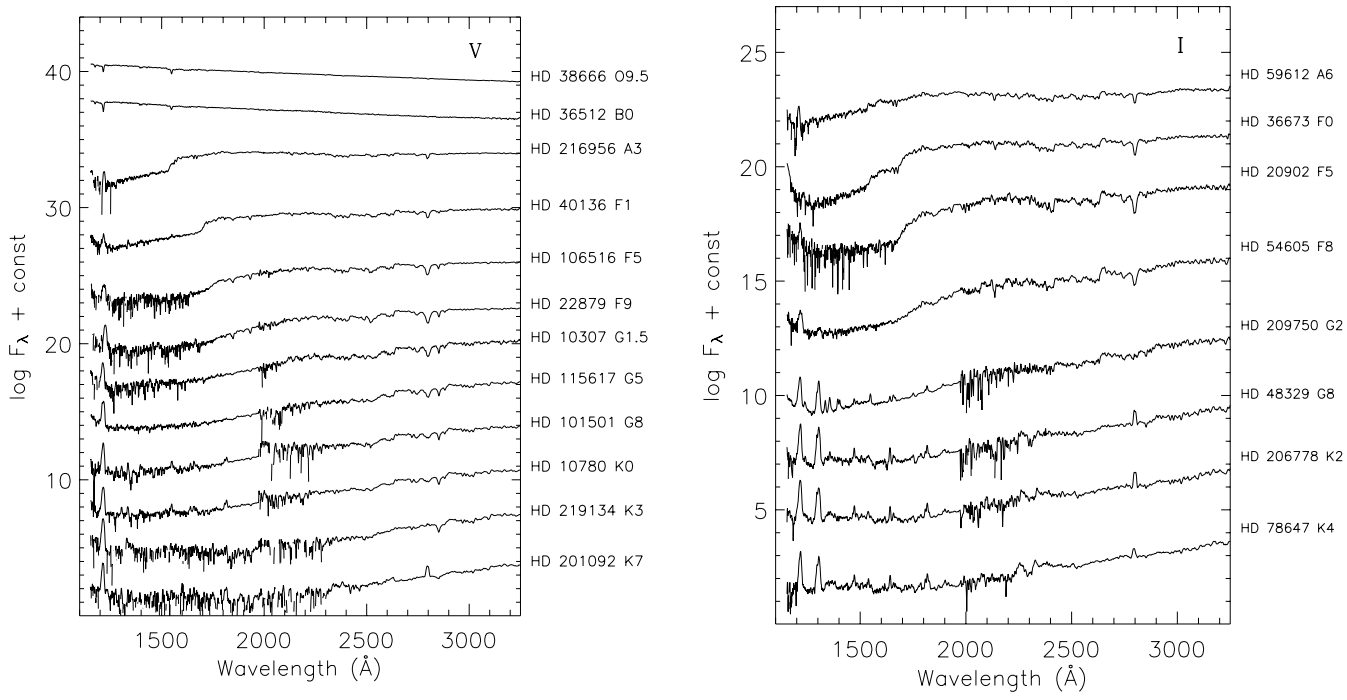

FIG. 9.—Illustrative selection of SEDs of the *IUE* atlas with luminosity class V (dwarfs) and I (supergiants).

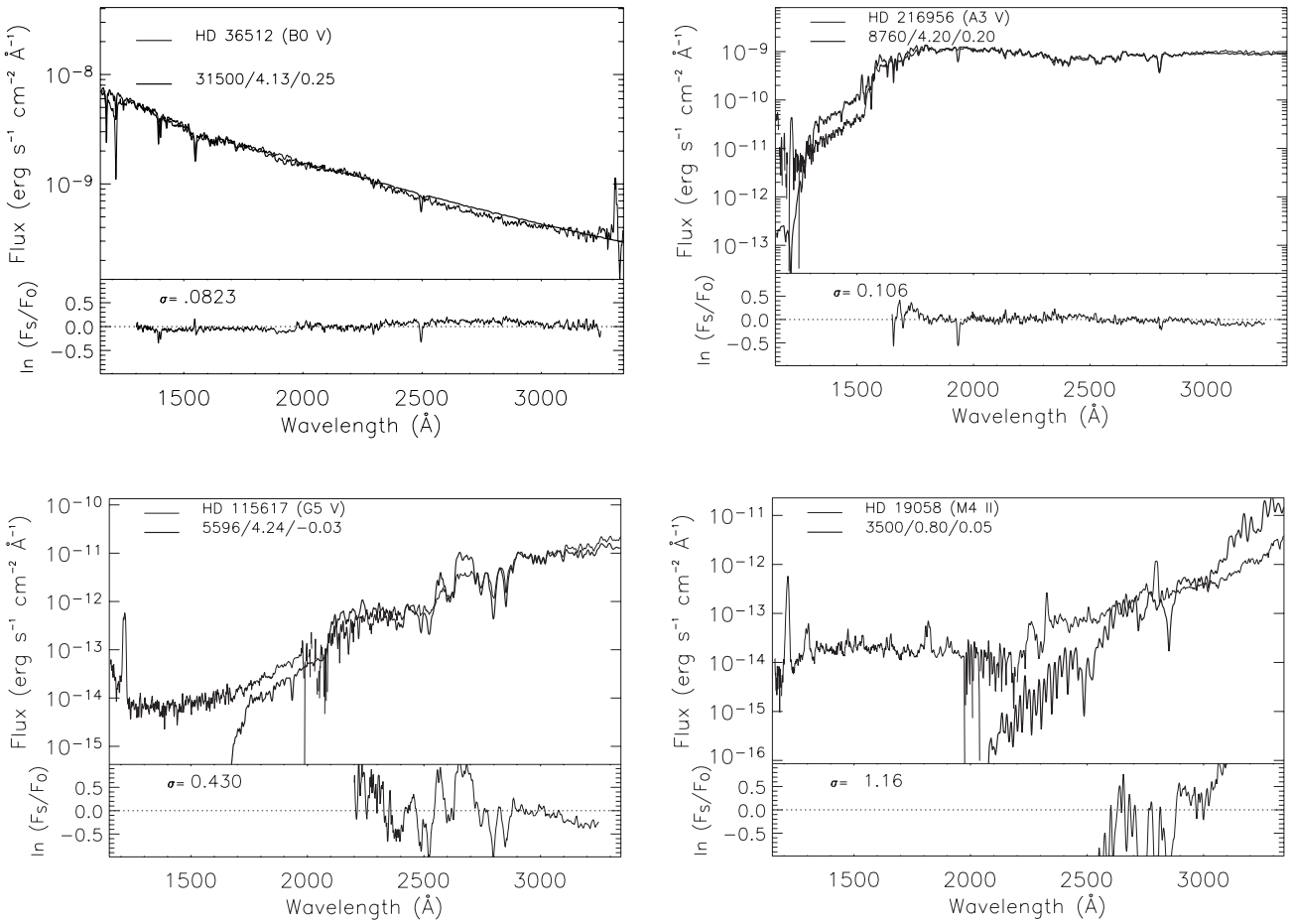

FIG. 10.—Example of our comparison procedure for a selected set of *IUE* stars of different spectral type. Theoretical fluxes have been scaled after a normalization such that $\langle \ln f(\lambda)_{\rm IUE} - \ln f(\lambda)_{\rm UVBLUE} \rangle = 0$.

thus suggesting a slightly warmer value for $T_{\rm eff}$ or enhanced continuum emission due to a chromosphere contribution.

c) *HD 195633*.—The UV spectrum of this G0 V star is clearly incompatible with its spectral type suggesting either a problem with its atmosphere parameters or, more likely, with the reddening correction (that in this case might have been underestimated).

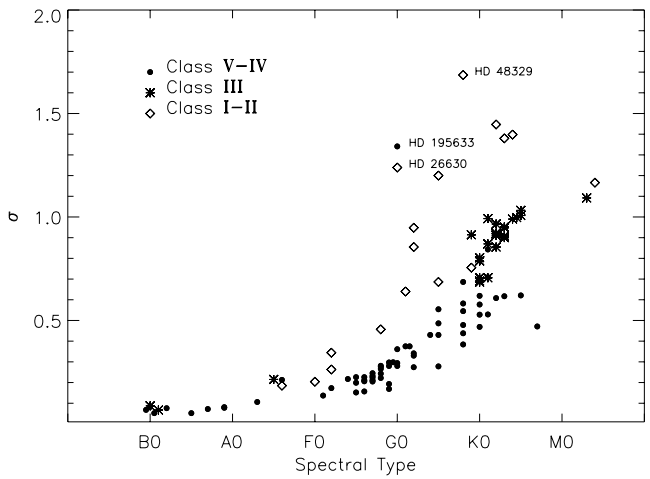

FIG. 11.—Comparison between observed and theoretical spectra can be summarized with this plot. Discrepancies are given by the standard deviation as a function of the spectral type (σ, see text). Three striking outliers are labeled in the plot with their HD number (see text for a discussion).

4. *Late-type stars: K and M*.—The UV spectra of these stars are dominated by chromospheric emission, and only the wavelength region redder than $\lambda \gtrsim 2900$ Å is usefully reproduced by theoretical models. The Mg II doublet is in strong emission for stars later than K2 III or K5 V, while the 2852 Å Mg I photospheric line is far more intense in theoretical spectra, especially for giants and supergiants (Fig. 10, *lower right panel*).

5. SUMMARY AND FUTURE WORK

We have built a new grid of theoretical fluxes, the UVBLUE library, at high resolution ($R = 50{,}000$) for a wide volume in the parameter space. The models suitably cover in the Hertzsprung-Russell diagram the full evolution of high- and low-mass stars and consist of nearly 1800 spectra spanning the wavelength region of 850–4700 Å, the most comprehensive ever computed at high resolution in the ultraviolet-blue spectral band. Unlike most empirical and theoretical libraries, UVBLUE includes all stellar types (with $T_{\rm eff}$ comprising between 3000 and 50,000 K), extending its applicability to the study of single stars and stellar systems through population synthesis models.

Work is in progress to extend the spectral coverage of the grid down to the He ionization edge, in the EUV range, and further explore the parameter space by including "Population III" stars at $[{\rm M/H}] \ll -2$, as well as a wider range of microturbulent velocity. The forthcoming implementation in our code of H_2 and

Lyα quasi-molecular H-H and H-H$^+$ opacities will also allow a substantial refinement in the calculation of far-UV synthetic spectra of intermediate-type stars. The recent analysis of Castelli & Kurucz (2001) indicates, in fact, that the lack of these opacities might explain the disagreement between observed and theoretical SEDS found in some metal deficient A-type stars.

In this work we have restricted our analysis just to the presentation of the new spectral grid and reviewed some relevant issues for a safe application of the theoretical models to UV observations. Our analysis also included a brief comparison of our LTE models with the corresponding output from the NLTE synthesis code TLUSTY. As expected, the match at low spectral resolution is fairly good (however, with NLTE models, slightly redder, on average, compared to the LTE SED for the same $T_{\rm eff}$), while a larger difference could be detected for weak lines that are nearly wiped out by the enhanced core emission component in case of NLTE atmospheres. These effects seem to magnify at metal-poor abundance (typically $[{\rm M/H}] \lesssim -1$).

A general comparison with UV observations has been carried out, mainly relying on the subset of stars of the Wu et al. (1983) and Fanelli et al. (1990) *IUE* catalog with complete atmosphere parameters available from the literature. A match with a working sample of 111 objects showed that UVBLUE models provide an accurate description of the main mid- and low-resolution spectral features for stars along the whole sequence from the B to $\sim$G5 type. The residual rms in our comparison procedure, however, sensibly degrades for later spectral types, with supergiant stars that are in general more poorly reproduced than dwarfs. As a possible explanation of the general trend, we point out that observations were compared with theoretical SEDs built up according to the fiducial atmosphere parameters provided by the literature, and *no* best fit was searched to the observations. This procedure is, obviously, prone to any uncertainty in the input set for $T_{\rm eff}$, log g, and [M/H], and in the reddening correction, both effects naturally reflecting in a poorer value of σ, via equation (1). In addition, one should also consider the important contamination of the *IUE* stellar atlas as a result of double or multiple stars and variability effects in most late-type objects. This clearly works in the sense of artificially worsening the match between theory and observations.

A parallel effort, aimed at constructing a cleaner and complete sample of normal stars from the *IUE* data, and self-consistently complementing the estimate of their atmosphere fundamental parameters, is in progress with new optical observations collected by our group at the "G. Haro" Observatory of Cananea (Mexico). A substantially improved agreement with the models should be expected for this better tuned stellar sample that, by the way, will also provide a valuable empirical atlas for reference in future studies.

These results will be the subject of a forthcoming paper in this series (M. Chavez et al. 2005, in preparation), where we will also approach in further detail the application of UVBLUE synthetic spectra to the analysis of UV narrowband indices like those of Fanelli et al. (1990). The further application of the UVBLUE library for high-resolution stellar population synthesis will be the natural next step in our work (A. Buzzoni et al. 2005, in preparation), relying on the Buzzoni (1989, 2002) theoretical code to have a deeper look at the main distinctive properties of galaxy SEDs.

The authors are pleased to thank Octavio Cardona at INAOE for fruitful discussions and helpful suggestions that accompanied our work along the entire UVBLUE project. We acknowledge financial support from Mexican CONACyT, via grant 36547-E, and Italian MURST, under grant COFIN00 02-016. M. C. would like to express his gratitude to the Vatican Observatory for partially supporting his sabbatical stay at the University of Arizona.

REFERENCES

Allende Prieto, C., Hubeny, I., & Lambert, D. L. 2003, ApJ, 591, 1192
Anders, E., & Grevesse, N. 1989, Geochim. Cosmochim. Acta, 53, 197
Barbuy, B., Perrin, M. N., Katz, D., Coelho, P., Cayrel, R., Spite, M., & Van't Veer-Menneret, C. 2003, A&A, 404, 661
Bertone, E., Buzzoni, A., Chavez, M., & Rodríguez-Merino, L. H. 2004, AJ, 128, 829
Blanco, C., Bruca, L., Catalano, S., & Marilli, E. 1982, A&A, 115, 280
Böhm-Vitense, E. 1958, Z. Astrophys., 46, 108
Böhm-Vitense, E., Mena-Werth, J., Carpenter, K. G., & Robinson, R. D. 2001, ApJ, 550, 457
Bouret, J.-C., Lanz, T., Hillier, D. J., Heap, S. R., Hubeny, I., Lennon, D. J., Smith, L. J., & Evans, C. J. 2003, ApJ, 595, 1182
Brandt, J. C., et al. 1998, AJ, 116, 941
Bressan, A., Chiosi, C., & Fagotto, F. 1994, ApJS, 94, 63
Brown, T. M., Ferguson, H. C., & Davidsen, A. F. 1996, ApJ, 472, 327
Bruzual, A. G., & Charlot, S. 2003, MNRAS, 344, 1000
Buzzoni, A. 1989, ApJS, 71, 817
———. 2002, AJ, 123, 1188
———. 2003, in ASP Conf. Ser. 297, Star Formation through Time, ed. E. Perez, R. M. Gonzalez Delgado, & G. Tenorio-Tagle (San Francisco: ASP), 471
Castelli, F., Gratton, R. G., & Kurucz, R. L. 1997, A&A, 318, 841
Castelli, F., & Kurucz, R. L. 2001, A&A, 372, 260
Cayrel de Strobel, G., Soubiran, C., Friel, E. D., Ralite, N., & François, P. 1997, A&AS, 124, 299
Cheng, K. P., & Neff, J. E. 2003, AJ, 125, 868
Diplas, A., & Savage, B. D. 1994, ApJS, 93, 211
Fanelli, M. N., O'Connell, R. W., Burstein, D., & Wu, C. 1990, ApJ, 364, 272
———. 1992, ApJS, 82, 197
Fitzpatrick, E. L., & Massa, D. 1999, ApJ, 525, 1011
Franchini, M., Morossi, C., & Malagnini, M. L. 1998, ApJ, 508, 370
Gardiner, R. B., Kupka, F., & Smalley, B. 1999, A&A, 347, 876
Girardi, L., Bressan, A., Bertelli, G., & Chiosi, C. 2000, A&AS, 141, 371
Glebocki, R., & Stawikowski, A. 2000, Acta Astron., 50, 509
Gonzalez Delgado, R. M., & Leitherer, C. 1999, ApJS, 125, 479
Gonzalez Delgado, R. M., Cerviño, M., Martins, L. P., Leitherer, C., & Hauschildt, P. H. 2005, MNRAS, 357, 945
González-Riestra, R., Cassatella, A., & Wamsteker, W. 2001, A&A, 373, 730
Gray, R. O., Graham, P. W., & Hoyt, S. R. 2001, AJ, 121, 2159
Gunn, J. E., & Stryker, L. L. 1983, ApJS, 52, 121
Gustafsson, B., Bell, R. A., Eriksson, K., & Nordlund, Å. 1975, A&A, 42, 407
Hauschildt, P. H., Starrfield, S., Shore, S. N., Allard, F., & Baron, E. 1995, ApJ, 447, 829
Holweger, H. 1970, A&A, 4, 11
Hubeny, I., & Lanz, T. 1992, A&A, 262, 501
Jacoby, G. H., Hunter, D. A., & Christian, C. A. 1984, ApJS, 56, 257
Kudritzki, R. P. 1976, A&A, 52, 11
Kudritzki, R. P., & Puls, J. 2000, ARA&A, 38, 613
Kurucz, R. L. 1979, ApJS, 40, 1
———. 1992, Rev. Mex. AA, 23, 45
———. 1993a, CD-ROM 13, ATLAS9 Stellar Atmosphere Programs and 2 km/s Grid (Cambridge: SAO)
———. 1993b, CD-ROM 18, SYNTHE Synthesis Programs and Line Data (Cambridge: SAO)
———. 1995, in ASP Conf. Ser. 81, Laboratory and Astronomical High Resolution Spectra, ed. A. J. Sauval, R. Blomme, & N. Grevesse (San Francisco: ASP), 583
Lanz, T., & Hubeny, H. 2003, ApJS, 146, 417
Le Borgne, J. F., et al. 2003, A&A, 402, 433
Leckrone, D. S., Johannson, S., Kurucz, R. L., & Adelman, S. J. 1990, in Atomic Spectra and Oscillator Strengths for Astrophysics and Fusion Research, ed. J. E. Hansen (Amsterdam: North Holland), 3
Leitherer, C., et al. 1999, ApJS, 123, 3

Mathis, J. S. 1990, ARA&A, 28, 37
Mihalas, D. 1972, ApJ, 176, 139
Moos, H. W., et al. 2000, ApJ, 538, L1
Morales, C., et al. 2000, ApJ, 530, 403
Morossi, C., Di Marcantonio, P., Franchini, M., Malagnini, M. L., & Chavez, M. 2002, ApJ, 577, 377
Parsons, S. B., & Ake, T. B. 1998, ApJS, 119, 83
Pellerin, A., et al. 2002, ApJS, 143, 159
Pettini, M. 2002, in New Quests of Stellar Astrophysics, ed. M. Chavez et al. (Dordrecht: Kluwer), 229
Pickles, A. J. 1985, ApJS, 59, 33
Salasnich, B., Girardi, L., Weiss, A., & Chiosi, C. 2000, A&A, 361, 1023
Schaerer, D., & de Koter, A. 1997, A&A, 322, 598
Uesugi, A., & Fukuda, I. 1982, Revised Catalogue of Stellar Rotational Velocities (Kyoto: Kyoto Univ. Dept. Astron.)
Vazdekis, A. 1999, ApJ, 513, 224
Walborn, N. R., Fullerton, A. W., Crowther, P. A., Bianchi, L., Hutchings, J. B., Pellerin, A., Sonneborn, G., & Willis, A. J. 2002, ApJS, 141, 443
Werner, K. 1988, A&A, 204, 159
Worthey, G. 1994, ApJS, 95, 107
Wu, C.-C., et al. 1983, The *IUE* Ultraviolet Spectral Atlas (Greenbelt: NASA)